Geophysical Research Letters

RESEARCH LETTER
10.1029/2023GL102974

Sediment Entrainment and Slump Blocks Limit Permafrost Riverbank Erosion

Madison M. Douglas[1], Kieran B. J. Dunne[1], and Michael P. Lamb[1]

[1]Division of Geological and Planetary Sciences, California Institute of Technology, Pasadena, CA, USA

Key Points:

- A new model shows that permafrost bank erosion depends both on pore ice thaw and sediment entrainment
- Sediment entrainment from thawed banks and slump blocks can be rate-limiting in some cases, which helps explain slow bank migration rates
- Where limited by sediment entrainment, decadal erosion rates may be less sensitive to warming river water than predicted previously

Supporting Information:

Supporting Information may be found in the online version of this article.

Correspondence to:

M. M. Douglas,
mmdougla@caltech.edu

Citation:

Douglas, M. M., Dunne, K. B. J., & Lamb, M. P. (2023). Sediment entrainment and slump blocks limit permafrost riverbank erosion. *Geophysical Research Letters*, *50*, e2023GL102974. https://doi.org/10.1029/2023GL102974

Received 23 JAN 2023
Accepted 19 MAY 2023

Abstract Climatic warming and permafrost thaw are predicted to increase Arctic riverbank erosion, threatening communities and accelerating sediment, carbon and nutrient cycling between rivers and floodplains. Existing theory assumes that pore-ice thaw sets riverbank erosion rates, but overpredicts observed erosion rates by orders of magnitude. Here, we developed a simple model that predicts more modest rates due to a sediment-entrainment limitation and riverbank armoring by slump blocks. Results show that during times of thaw-limited erosion, the river rapidly erodes permafrost and undercuts its banks, consistent with previous work. However, overhanging banks generate slump blocks that must thaw and erode by sediment entrainment. Sediment entrainment can limit bank and slump block erosion rates, producing seasonally averaged rates more consistent with observations. Importantly, entrainment-limited riverbank erosion does not depend on water temperature, indicating that decadal erosion rates may be less sensitive to warming than predicted previously.

Plain Language Summary Riverbank erosion in the Arctic is a major hazard for riverside communities and infrastructure. Arctic rivers flow through regions of permanently frozen ground, and this ground is thawing as the climate warms. Therefore, there is major concern that riverbank erosion will accelerate in the future because the ground loses its strength when thawed. However, in order for a riverbank to erode, the river must satisfy two conditions: it must thaw the frozen ground and entrain the thawed sand and mud. Our model and analyses suggest that riverbank erosion in many Arctic rivers can be limited by the river's ability to entrain and transport the sand and mud, rather than the canonical view that erosion is limited by the rate of ground thaw. Applying our model to the Yukon River indicates that thaw rates are so fast that they cannot set the rate of erosion for the melt season. Instead, bank erosion for part of the time is controlled by the ability of the river to move the bank sediment, making riverbank erosion less sensitive to warming river waters.

1. Introduction

Major river systems flow through the Arctic, contributing approximately 10% of freshwater and 1% of sediment flux to Earth's oceans (Gordeev, 2006). These rivers flow through permafrost regions, which contain a seasonally thawed active layer underlain by frozen ground (Obu et al., 2019). Arctic rivers can migrate rapidly (Rowland et al., 2019), eroding floodplain material that affects the carbon cycle (Turetsky et al., 2020) and threatens riverside communities and infrastructure (Bronen & Chapin, 2013; UAF & USACE, 2019).

Riverbank erosion in permafrost is thought to be limited by rates of pore-ice melting, implying that erosion rates could dramatically increase as the climate warms (Costard et al., 2003). This theory matches observed erosion rates along the Lena River in Siberia of 2–40 m/yr during the period after river ice break-up (Costard et al., 2014). However, Costard et al. (2014) only modeled erosion through the end of June, when predicted erosion rates approached 6 m/day. If the same 6 m/day rate applies until freeze-up in the fall, the model predicts over 500 m/yr of erosion, an order of magnitude greater than the fastest observed rates. Therefore, there must be a mechanism that substantially reduces bank erosion rates from the thaw-limited case.

Here we explore two mechanisms that might slow seasonally averaged permafrost bank erosion rates compared to the thaw-limited end-member. Field studies of permafrost rivers in late summer show that banks have an order-meter-thick layer of thawed sediment at their surface (Scott, 1978), indicating erosion was limited by the river's ability to entrain sediment from the bank (i.e., entrainment-limited bank erosion) rather than being limited by pore-ice thaw. In addition, bank undercutting and slump block generation is common in Arctic rivers (Figure 1). These blocks can prevent further bank erosion until the fallen material has been entrained and transported downstream. We incorporate these two mechanisms into a model for riverbank erosion and discuss their implications for the fate of rivers in a warming Arctic.

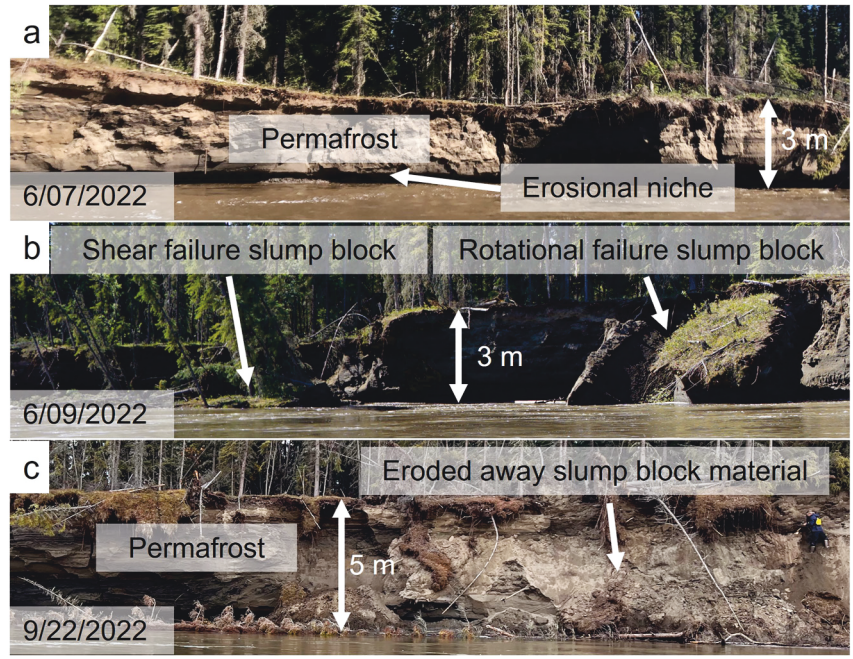

Figure 1. Field photos of the same permafrost river bank near Beaver, AK (66.3316°N, 147.6156°W) taken on different dates. Bank stands approximately 3.5 m above the water level. The majority of exposed bank face is permafrost with pore ice. The active layer on top of the bank is between 0.5 and 1 m deep. (a) Flowing water undercut the bank, creating an erosional niche (07 June 2022). (b) Shear failure and rotational failure-generated slump blocks (09 June 2022). (c) Slump block material armors the bank and prevents the development of an erosional niche until the material has been eroded away (22 September 2022). Photo Credit: Kieran Dunne (a, c), Michael Lamb (b).

2. Model Development

We developed a 2D model for permafrost riverbank erosion where erosion rates may be thaw- or sediment entrainment-limited, and bank erosion only occurs when the permafrost bank is not shielded by slump blocks (Figure 2). The model was motivated by field observations near Beaver, AK in summer 2022. In the early summer following ice break-up, we observed that permafrost banks were often undercut by meter-deep

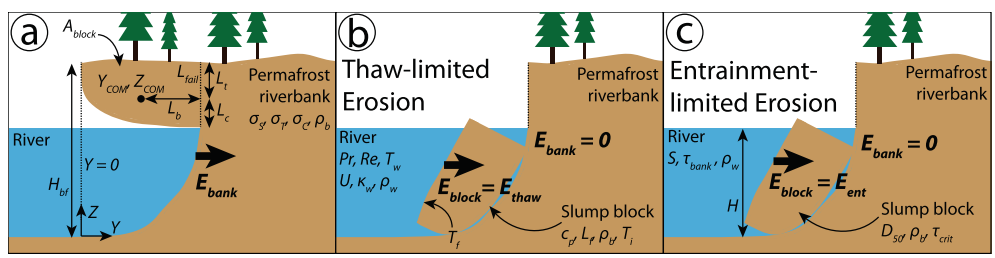

Figure 2. Illustration of the permafrost riverbank erosion model setup. (a) We define a coordinate system where the bank erodes horizontally from an initial position of $Y = 0$ m and elevation is measured from the channel thalweg ($Z = 0$ m) to the top of the bank ($Z = H_{bf}$ m). The riverbank erodes below the water surface at an erosion rate (E_{bank}; m/s) equal to the minimum of the thaw-limited (E_{thaw}; m/s) and entrainment-limited (E_{ent}; m/s) erosion rates. The bank overhang has a total failure plane length (L_{fail}; m) with sections under tension (L_t; m) and compression (L_c; m); area of the overhang A_{block} (m^2); distance L_b (m) from the block center of mass at (Y_{COM}, Z_{COM}) to the failure plane; and permafrost bulk density (ρ_b; kg/m^3), shear strength (σ_S; Pa), tensile strength (σ_T; Pa), and compressive strength (σ_C; Pa). When slump blocks are present, $E_{bank} = 0$ and the block is eroded at rate E_{block} (m/s), which may be (b) thaw-limited or (c) entrainment-limited. (b) E_{thaw} depends on the river Prandtl number (Pr; dimensionless), Reynolds number (Re; dimensionless), mean flow velocity (U; m/s), temperature (T_w; °C), thermal conductivity (κ_w; W/m/K), density (ρ_w; kg/m^3), and temperature of fusion (T_f; °C); as well as permafrost temperature (T_i; °C), specific heat capacity (c_p; J/kg/°C), and latent heat of fusion (L_f; J/kg). (c) E_{ent} depends on the shear stress on the bank (τ_{bank}; Pa), which depends on the water depth (H; m) and channel slope (S; m/m); the slump block median grain size (D_{50}; m); and the critical shear stress to entrain bank material (τ_{crit}; Pa).

erosional niches (Figure 1a). Rotational and shear failure generated slump blocks approximately 3–7 m wide along the bank (Figure 1b). Permafrost banks without erosional niches typically showed armoring from thawed remnants of previous bank failures, suggesting erosion was limited by sediment entrainment (Figure 1c).

We modeled the instantaneous riverbank erosion rate E_{bank} (m/s) as the minimum of thaw-limited (E_{thaw}; m/s) and sediment-entrainment-limited erosion rates (E_{ent}; m/s):

$$E_{\text{bank}} = \min(E_{\text{thaw}}, E_{\text{ent}}) \tag{1}$$

We calculated E_{thaw} using the model of Costard et al. (2003) with thermal properties for saturated permafrost calculated following Dupeyrat et al. (2011):

$$E_{\text{thaw}} = \frac{APr^{\alpha}Re^{\beta}\kappa_w(T_w - T_f)}{H\rho_b(L_f + c_p(T_f - T_i))} \tag{2}$$

where the numerator is the rate of heat transfer from the river water to the bank and the denominator is the heat required to thaw the bank. In Equation 2, A, α, and β are empirical coefficients; $\text{Pr} = \nu/\chi$ is the Prandtl number, where ν (m^2/s) is the kinematic viscosity and χ is the thermal diffusivity (m^2/s) of water; $\text{Re} = HU/\nu$ is the Reynolds number, where U (m/s) is the mean river flow velocity; κ_w (W/m/°C) is water thermal conductivity; T_w is river water temperature (°C); T_f (°C) is the freezing point of water; H (m) is the flow depth; ρ_b (kg/m^3) is permafrost bulk density; L_f (J/kg) is permafrost latent heat of fusion; c_p (J/kg/°C) is permafrost heat capacity; and T_i (°C) is the initial temperature of floodplain permafrost. We calculated $L_f = f_{\text{ice}}L_{\text{ice}}$, where f_{ice} (kg/kg) is the mass fraction of water ice in permafrost and L_{ice} (J/kg) is the water ice latent heat of fusion.

We modeled E_{ent} using a threshold-based model after Partheniades (1965),

$$E_{\text{ent}} = \frac{M}{\rho_b f_{\text{sed}}}\left(\frac{\tau_{\text{bank}}}{\tau_{\text{crit}}} - 1\right)^n \tag{3}$$

where M ($kg/m^2/s$) and n (dimensionless) are empirical coefficients, τ_{bank} (Pa) is the fluid shear stress on the bank, τ_{crit} (Pa) is the critical shear stress to entrain bank sediment, and f_{sed} (kg/kg) is the mass fraction of sediment: $f_{\text{sed}} = 1 - f_{\text{ice}}$. We do not include detailed calculations on the river bend geometries or hydraulics, which would modify τ_{bank} for any given bend.

We implemented the erosion equations for a 2-D cross-sectional elevation profile of a riverbank, tracking the water depth, H, throughout an annual hydrograph (see Section 3). The river has a bankfull depth of H_{bf} (m), and we defined a vertical coordinate system with the river thalweg at $Z = 0$ and the top of the bank at $Z = H_{\text{bf}}$. At each time step, the bank was eroded horizontally (in the positive Y direction) at the rate E_{bank} (Equation 1) using finite differences everywhere on the submerged portion of the bank ($Z < H$) (Figure 2).

As the bank erodes during falling water level, the model generates overhangs that fail, producing slump blocks. We assessed bank failure following Patsinghasanee et al. (2018), which allows for rotational and shear failure of overhangs along a vertical plane (Figures 2b and 2c). We calculated the factor of safety (F_s) as the maximum of the factor of safety for rotational failure ($F_{s,\text{rot}}$; dimensionless) and shear failure ($F_{s,\text{shear}}$; dimensionless):

$$F_s = \max(F_{s,\text{rot}}, F_{s,\text{shear}}) \tag{4}$$

where $F_s > 1$ indicates that the driving forces exceed the bank strength and failure occurs. For rotational failure,

$$F_{s,\text{rot}} = \frac{2\rho_b g A_{\text{block}} L_b}{\sigma_C L_c^2 + \sigma_T L_t^2} \tag{5}$$

where g is gravitational acceleration (9.81 m/s^2); σ_C (Pa) and σ_T (Pa) are the compressive and tensile strengths of permafrost, respectfully; L_c (m) and L_t (m) are the lengths of the failure plane under compressive stress and tensile stress, respectfully; and L_b (m) is the horizontal distance from the slump block's center of mass (Y_{COM}; m) to the failure plane. We assumed that the failure plane is vertical and occurs in the subaerial portion of the overhanging bank, such that $L_{\text{fail}} = H_{\text{bf}} - H$ at the time of failure (Figure 2a). Thus, $L_t = H_{\text{bf}} - Z_{COM}$, where

Z_{COM} (m) is the height of the slump block's center of mass, and $L_c = L_{fail} - L_t$. The factor of safety for shear failure was calculated from the weight of the block divided by block shear strength (σ_S; Pa) along the failure plane:

$$F_{s,shear} = \frac{\rho_b g A_{block}}{\sigma_S L_{fail}}. \quad (6)$$

The cross-sectional area of the failed block, A_{block}, was found by integrating the bank profile elevation above the water line to the failure plane (Figure 2a).

To implement bank failures in our model, at each timestep, we evaluated if bank failure occurred using Equations 4–6. If failure occurred ($F_s > 1$), the overhanging material was removed from the bank cross-sectional profile, a slump block was generated, and the slump block was assumed to armor the bank and protect it from erosion ($E_{bank} = 0$ when $E_{block} > 0$). Slump block material was tracked separately from the bank and eroded at a rate E_{block} (m/s), which was either thaw- or entrainment-limited such that

$$E_{block} = \min(E_{thaw}, E_{ent}) \quad (7)$$

with E_{thaw} and E_{ent} evaluated using Equations 2 and 3. We assumed that the block was fully submerged and eroded from an initial area A_{block} at rate $E_{block}H$. After the slump block was eroded away, $E_{block} = 0$, and E_{bank} was assessed again using Equation 1. We calculated the mean annual erosion rate E_{avg} (m/yr) as the total area of bank and block material eroded over the year normalized by H_{bf}.

3. Model Implementation

We used input values for the model based on the Yukon River between Stevens Village, AK and Beaver, AK as an example case (Table S1 in Supporting Information S1). Here the river traverses discontinuous permafrost and transitions from an anabranching to single-threaded channel morphology. The channel is gravel-bedded ($D_{50} \sim 10$ mm) with slope $S = 1.6 \times 10^{-4}$ (Clement, 1999). However, not all model parameters are known for this site, nor was the model locally calibrated. Our goal is to show an illustrative example of model behavior, not predictive results for any given river bend.

We used water discharge and temperature data from USGS gage 15453500 near Stevens Village. The daily discharge timeseries spans 1976–present and water temperature data exist intermittently from 1970 to 2005. We produced a representative annual timeseries of water velocity and depth from the discharge timeseries using power law fits to available paired measurements (Figure S1 in Supporting Information S1). An average annual daily water temperature timeseries was found by combining sparse water temperature measurements from Steven's Village ($n = 214$) with daily water temperature measurements from nearly Pilot Station, AK (USGS gage 15565447). We computed the median water temperature for each day of the year where data are available then smoothed the data using a Savitzky-Golay filter. Water temperature was set to 0°C for days in the spring with no available measurements, likely during ice breakup (Figure S1 in Supporting Information S1).

We assumed bankfull depth equals the median annual maximum flow depth of 9.8 m. The shear stress on the bank (τ_{bank}) was calculated as $\tau_{bank} = \tau_{bed}/(1 + \varepsilon)$, with $\varepsilon = 0.2$ (Parker, 1978). We assumed normal flow conditions, so that $\tau_{bed} = \rho_w gHS$, where ρ_w (kg/m^3) is the density of water.

We modeled a representative sandy permafrost riverbank ($D_{50} = 1$ mm). The initial condition was a vertical cutbank. We followed Costard et al. (2014) and used empirical coefficients of $A = 0.0078$, $\alpha = 0.3333$, $\beta = 0.9270$ (Equation 2) from experiments by Lunardini (1986), and set Pr = 10. Using values typical for permafrost, we set $T_f = 0$°C, $\sigma_C = 11.2 \pm 4.1$ MPa (±1SD) and $\sigma_T = 2.4 \pm 0.2$ MPa (±1SD) for frozen silt and sand (Bragg & Andersland, 1981; Wolfe & Thieme, 1964), and $\sigma_S = 5 \times 10^4$ Pa (Arenson & Springman, 2005). We used measured values of $\rho_b = 861$ kg/m^3 and $f_{ice} = 0.2362$ for soils in the study region (Lininger et al., 2019). Background permafrost temperature, $T_i = -1$°C, was determined from borehole data for Stevens Village at 3 m depth (Biskaborn et al., 2015). For sediment entrainment, we used $n = 1$ (Partheniades, 1965) and $M = 2.5 \times 10^{-5}$ kg/m^2/s to represent river sediment with some cohesion (Winterwerp et al., 2012). We calculated $\tau_{crit} = 0.28$ Pa for $D_{50} = 1$ mm (Parker et al., 2003).

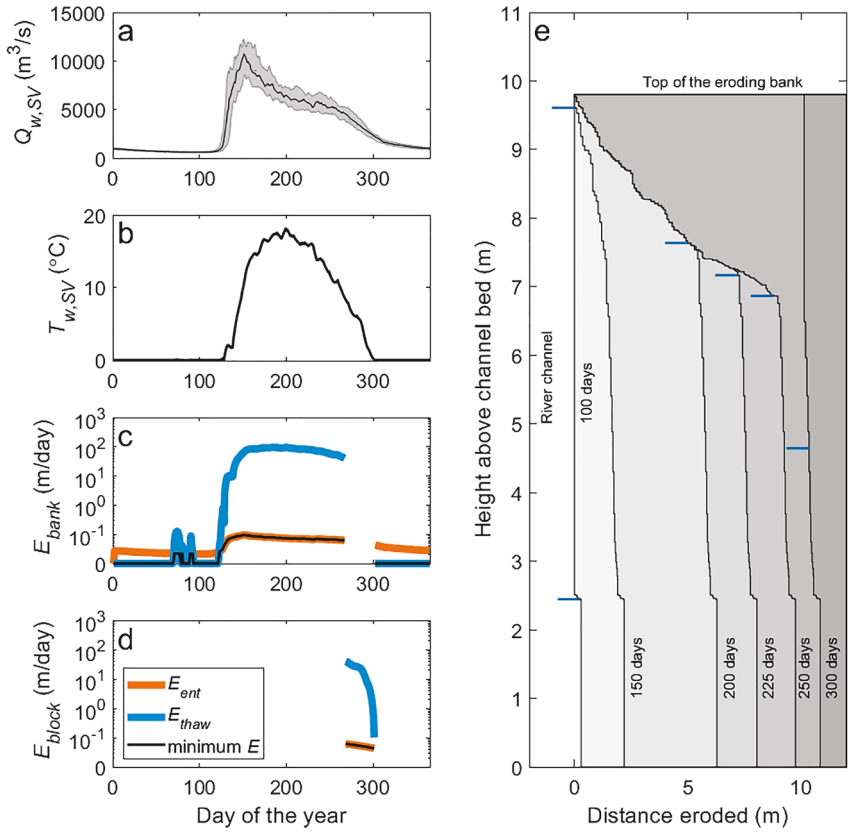

Figure 3. Riverbank erosion over the course of an annual hydrograph for sandy permafrost near Stevens Village along the Yukon River. (a) Median daily water discharge (Q_w; m^3/s) with the 25th to 75th percentiles shaded in gray (days since 01 January). (b) Median daily water temperature (T_w; °C) for Stevens Village and Pilot Station. (c) Riverbank erosion rate (E_{bank}; m/day), with E_{ent} and E_{thaw} shown in orange and blue, respectively. Bank erosion is zero when a slump block shields the bank. (d) Model of slump block erosion rate (E_{block}; m/day), E_{ent}, and E_{thaw} versus day of the year. (e) Eroding riverbank profiles shaded light to dark gray through time with water level shown as a blue dash on each profile.

4. Results

4.1. Yukon River Example Case

High water discharge for a typical hydrograph on the Yukon River near Stevens Village begins following ice breakup (day 120) and peaks around day 150 (since 01 January), before slowly declining to freeze-up around day 300 (Figure 3a). The water temperature gradually increases after ice breakup, peaking at a value of approximately 18°C in mid-summer (around day 200) before declining back to 0°C in the winter (Figure 3b). With these inputs, the model produces daily riverbank erosion rates (E_{bank}; Figure 3c) that are thaw-limited throughout the winter and the earliest part of the melt season (approximately 5 days) when the river water is cold ($T_w < 0.1$°C). After day 125, the thaw rate accelerates as the water warms, making bank erosion limited by sediment entrainment, rather than thaw, despite the rise in water discharge and the increase in entrainment rate. The bank remains entrainment-limited until day 300, shortly before freeze-up. Erosion rates closely track water discharge, and are relatively insensitive to water temperature during summer months when rates are set by sediment entrainment. While a small fraction of bank erosion occurs under thaw-limited conditions (<1%), permafrost still plays a crucial role in preventing erosion from occurring during winter months when $T_w = 0$°C. During this time, the river would entrain sediment if it was thawed, but temperatures are too low to permit thaw.

Rising and falling water levels form an overhang in the permafrost which collapses to form a slump block whose geometry is visible in plots of the riverbank profile through time (Figure 3e). The model produces bank profiles with a curved overhang reaching to the recent high-water level, similar to natural overhangs (Figure 1). Over the melt season, the model predicts one bank collapse event due to shear failure with a 10-m top length, consistent in scale with observed slump blocks. The slump block causes E_{bank} to vanish and E_{block} to abruptly increase while

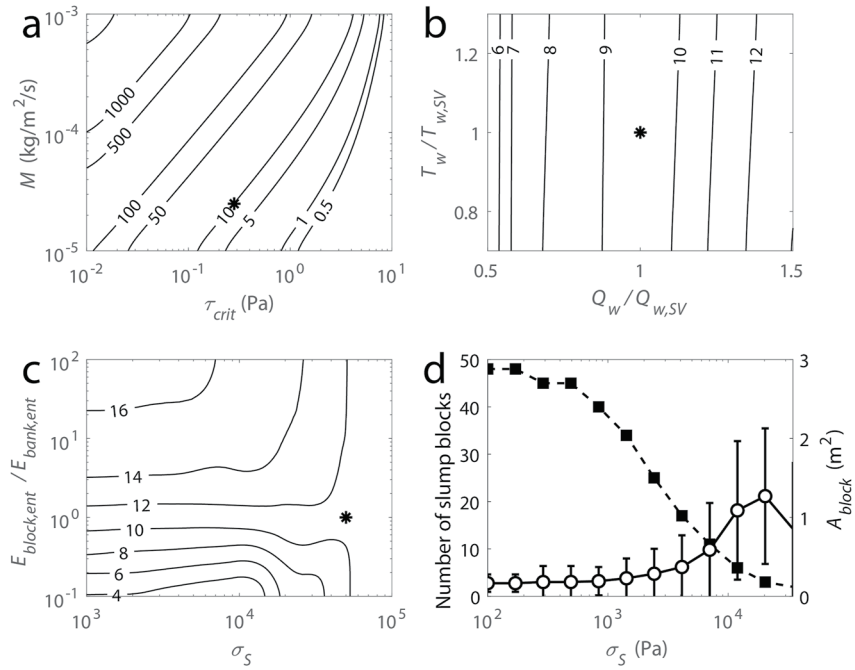

Figure 4. Contour plots of mean annual erosion rate E_{avg} (m/yr) smoothed with a 2-D Gaussian filter with 1SD = 0.05 and the modeled example case displayed as a star (*). (a) E_{avg} contours for changing sediment entrainment coefficient M and τ_{crit}. (b) E_{avg} contours for changes in the magnitude of water temperature and discharge. (c) E_{avg} contours for the ratio of block versus bank M and bank shear strength. (d) The number of slump blocks (black squares) and slump block area (white circles with 1SD error bars) as a function of bank shear strength.

bank material is protected by the slump block (Figures 3c and 3d). The slump block shields the bank from direct erosion for 39 days, persisting because water levels are decreasing, which makes block erosion less efficient. The block has a large area because L_{fail} is set by the subaerially exposed portion of the bank that generates failures. Block erosion is limited by the rate of sediment entrainment because it occurred as the hydrograph is declining and water temperatures are warm, so permafrost thaw rates are rapid (Figure 3d).

For our example scenario, the thaw-limited model (Equation 2) alone produces a mean annual bank erosion rate greater than 8×10^3 m/yr, which is not realistic. Allowing both thaw- and entrainment-limited erosion and slump block armoring of the bank predicts 10 m/yr of riverbank erosion. For comparison, reach-averaged values derived from Landsat imagery indicate erosion rates of 1.48 ± 2.73 m/yr (mean ± 1SD) and a maximum of 36.04 m/yr for the Yukon River between Beaver and Stevens Village (Rowland et al., 2019). Thus, the example scenario produces erosion rates that fall within the range of observed rates and represent an improvement by multiple orders of magnitude compared to assuming thaw-limited conditions. The exact erosion rates are sensitive to model input parameters, which we explore next.

4.2. Model Sensitivity Analysis

We systematically changed the thaw and entrainment-limited erosion rate coefficients while holding all other parameters constant. Entrainment rates are highly variable (de Leeuw et al., 2020) and depend on the particle size, sediment cohesion, and vegetation that can bind sediment. The Yukon River floodplain is poorly sorted, with grain size ranging from pebbles ($\tau_{crit} \sim 10$ Pa) to cohesive silt and clay ($\tau_{crit} \sim 0.01$ Pa), so we varied M and τ_{crit} over a wide range of values that are representative of the natural variability for these materials (Parker et al., 2003; Winterwerp et al., 2012). When entrainment rates are very low, the river rapidly switches from thaw- to entrainment-limited erosion and the number of days with thaw-limited erosion decreases (Figure 4a). In contrast, when sediment is easily entrained, the number of days with thaw-limited bank erosion increases and E_{avg} increases. The E_{avg} contours are not linear in log-log space because changing E_{ent} also changes the number of days when thaw-limited erosion occurs. The interplay between rates of thaw- and entrainment-limited erosion and number of days in each state provides a negative feedback on E_{avg} that limits runaway permafrost thaw or

sediment entrainment. Overall, these results suggest that the model produces erosion rates consistent with the observations (2–3 m/yr) depending on the values of M and τ_{crit}, which are poorly constrained. Changing coefficients A and β in the permafrost thaw model, or permafrost temperature, over a range of reasonable values had little effect on the model results for this scenario since the thaw-limited conditions were brief (Figures S2 and S3 in Supporting Information S1).

Water discharge and temperature are increasing as the climate warms (Docherty et al., 2019; Peterson et al., 2002). To investigate potential climatic changes, we ran model scenarios multiplying the Stevens Village water discharge timeseries ($Q_{w,SV}$) and the water temperature timeseries ($T_{w,SV}$) by a dimensionless scalar ranging from 0.5–1.5 to 0.7–1.3, respectively (Figure 4b). These ranges exceed observed variations in Arctic river discharge over the last 7 kyr (Wagner et al., 2011) and span modern river water temperatures for Arctic and temperate climates (Wanders et al., 2019). Model results indicate bank erosion rates increase with greater water discharge but are insensitive to water temperature. These trends emerge because permafrost riverbank erosion is only thaw-limited during summer months for a short period immediately after ice break-up, and otherwise bank erosion is entrainment-limited (Figure 4b). Bank and slump block erosion rates increase rapidly with respect to water discharge because both thaw- and entrainment-limited erosion rates depend on discharge (Figure 4b). Thaw-limited erosion rates are proportional to flow velocity (Equation 2) while entrainment-limited erosion rates are proportional to flow depth via shear stress (Equation 3), which both increase with discharge. In addition, more of the bank is exposed to erosion at higher water depths.

Slump block material may be more or less erodible relative to the underlying bank (Parker et al., 2011). For instance, slump blocks could be easier to erode because they have more surface area exposed to flow, they are comprised of weaker material, or the blocks break apart during failure. In contrast, slump blocks might be more difficult to erode than their underlying bank because they contain finer, more cohesive sediment and organics such as tree roots from the upper floodplain. To understand these effects, we multiplied entrainment-limited erosion rates by a dimensionless scalar from 0.1 to 10 (simulating blocks that range from 10% to 10-fold the strength of the bank material) and examined how bank erosion rates varied with block erodibility and bank shear strength (Figure 4c). Intuitively, E_{avg} increased when slump blocks were easier to erode than their underlying material and decreased when slump blocks were more difficult to erode (Figure 4c). Therefore, the presence of cohesive materials, such as mud and plant roots, within slump blocks provides an additional mechanism to slow bank erosion rates, consistent with non-permafrost rivers (Parker et al., 2011). In our modeled scenarios, most slump blocks were eroded under entrainment-limited conditions, thus the results are not strongly affected by whether or not the slump block was initially frozen.

Since bank failures in our modeled scenarios were due to shear rather than rotational failure, we explored the effect of changing shear strength on model results. We examined a broad range of strengths (σ_S = 1–1,000 kPa): laboratory values give a range over multiple orders of magnitude for frozen sand with varying ice content and temperature (Arenson & Springman, 2005), and observations of overhanging, vertical, and low-angle banks imply bank strength spans a wide range of values. Overall, higher σ_S decreases the number of slump blocks and increases their size (Figure 4d). This occurs because a weaker bank requires less of an overhang to form before it fails, producing numerous small collapses over the course of the summer, while stronger banks need large overhangs to form before bank shear strength is exceeded. Despite shear strength strongly affecting the number of slump blocks and their residence time, it has a small effect on mean annual erosion rates when blocks have similar erodibility as the banks (Figure 4c). Slump blocks instead modulate the instantaneous rate of bank erosion, rather than the mean annual bank erosion rate. However, when blocks are resistant to entrainment, erosion rates first increase then decrease as shear strength increases. In contrast, for blocks that are highly erodible, average bank erosion rates first decrease then increase as shear strength increases. This occurs because increasing bank strength makes slump block failures occur later in the summer, and slump blocks that cover the bank when erosion rates peak during in early summer will most significantly increase (for weak blocks) or decrease (for strong blocks) annual erosion rates.

5. Discussion

Our model indicates slump blocks and entrainment-limited conditions can help to explain overestimates of permafrost riverbank erosion by thaw-limited theory. Using simple block collapse and sediment entrainment formulations, the model produces erosion rates similar to observations along the Yukon River. The model is

simple by design to illustrate the important role that sediment entrainment and slump blocks play in modulating thaw-induced bank erosion rates. A predictive model may require additional physical processes, for instance, bank gouging by ice jams (Vandermause et al., 2021). In addition, our model does not track heat transferred to the bank during periods of entrainment-limited erosion. This may be important because sustained low flows could thaw the bank, allowing for rapid erosion during late-summer floods (McNamara et al., 2008). In addition, bank thaw may cause permafrost with very high pore-ice content to collapse, increasing erosion rates compared to our model. We also neglected form drag from slump blocks and fallen trees (Figure 1), which could slow near-bank flow, reducing bank shear stresses and erosion rates (Kean & Smith, 2004). Finally, our model neglects channel bend, bed, and bar morphodynamics, which can change bank stresses and modulate bank erosion rates on seasonal and inter-annual timescales (Naito & Parker, 2019, 2020).

Model results qualitatively match field observations, producing rapid, thaw-limited erosion in early summer and slower, entrainment-limited erosion with a large slump block as river discharge declines in mid- to late summer (Figure 1). Importantly, entrainment-limited erosion slows bank erosion by two orders of magnitude, while slump block armoring changes erosion rates when slumped material is more or less resistant to entrainment than the underlying bank. Erosion was entrainment-limited for $T_w > 0.1$°C, indicating that even catchments in continuous permafrost could be entrainment-limited for summer months. Since entrainment is important in setting the erosion rate, permafrost bank erosion in some rivers may behave more similarly to rivers in non-permafrost settings than previously thought.

Previous efforts to understand the effects of permafrost on channel mobility indicate that rivers are capable of rapidly eroding banks locally (Fuchs et al., 2020; Kanevskiy et al., 2016) yet erode more slowly when averaged spatially over river reaches and temporally over decadal timescales (Rowland et al., 2019). Spatial heterogeneity in riverbank and slump block strength and erodibility as well as channel hydraulics and curvature may account for some of these differences (Sylvester et al., 2019). Unfortunately, many of these parameters are poorly constrained for permafrost and non-permafrost rivers alike (Arenson & Springman, 2005; Bragg & Andersland, 1981; Wolfe & Thieme, 1964). For example, entrainment relations in non-permafrost settings commonly overpredict erosion rates, leading to proposals that plants, cohesive mud, or muddy slump blocks play important roles in throttling bank erosion rates (Parker et al., 2011). In addition, the interplay of thaw- and entrainment-limited erosion and the number of days per year that each process dominates may produce localized, rapid erosion over a few days following ice break-up but little to no erosion over the rest of the year, potentially reconciling fast short-term and slow long-term erosion rates along Arctic rivers. Thus, by allowing mixed entrainment-limited and thaw-limited behavior over the melt season, our model might help to reconcile observations of thaw-limited behavior (e.g., erosion rates depend on water temperature or pore ice content) with much slower averaged rates than predicted by purely thaw-limited conditions.

Arctic warming is increasing surface water temperatures (Docherty et al., 2019) and changing riverine hydrographs (Peterson et al., 2002). Our results show that, where partially entrainment limited, river morphodynamics may be less sensitive to warming of river water if thaw-limited conditions only persist for a few days after ice break-up, as in our modeled scenario. Moreover, thaw rates should increase with warming water temperature, which would result in them outpacing entrainment rates more often, further limiting the days in which erosion is thaw-limited. However, even if bank erosion rates are set by sediment entrainment, Arctic rivers will still respond to climate change through changing hydrographs. Increases in discharge and the size and frequency of late-summer storms, when riverbanks are thawed, can increase erosion rates (McNamara et al., 2008). Permafrost riverbanks also differ from non-permafrost banks because thaw rates are negligible during winter months, since water temperatures remain close to 0°C. As ice breakup occurs earlier in the year (Beltaos & Burrell, 2021), we expect that the number of days with non-zero erosion will increase, raising average annual erosion rates even if daily rates remain similar. Finally, regional permafrost thaw should reduce riverbank strength, resulting in smaller and more frequent slump blocks. Taken together, these changes may increase bank erosion hazards and change that cadence of cycling of floodplain materials including sediment, carbon, and pollutants.

6. Conclusions

Arctic rivers can erode rapidly, damaging infrastructure and forcing some communities to relocate. Understanding the physical processes that govern permafrost bank erosion is a crucial step toward predicting and mitigating hazards from climate change. Here, we introduced a model that includes thaw-limited permafrost erosion as well

as limits on erosion rates through slump block failure and sediment entrainment. The purely thaw-limited model produces unrealistically large erosion rates. However, simple representations of sediment entrainment and slump blocks reduce these rates by orders of magnitude, making predictions more comparable to observations. We also found that entrainment-limited conditions can occur over most of the summer in some cases, such that permafrost riverbank erosion can be sensitive to changes in water discharge but not water temperature. However, even in these scenarios, riverbank erosion may still accelerate if a warming climate leads to larger floods, potentially increasing hazards to riverside communities and the release of carbon currently stored in permafrost.

Conflict of Interest

The authors declare no conflicts of interest relevant to this study.

Data Availability Statement

Soil bulk density and water content data were downloaded from https://doi.org/10.25675/10217/187212. Data for ground temperature were downloaded for site ID US O-82 from the Global Terrestrial Network for Permafrost (GTN-P) Database at http://gtnpdatabase.org/boreholes. Yukon River temperature and discharge data were downloaded from https://waterdata.usgs.gov/monitoring-location/15565447/ and https://waterdata.usgs.gov/monitoring-location/15453500/. Model code was written in Matlab R2022a under an academic license to the California Institute of Technology and code to run the model is available on Zenodo at https://doi.org/10.5281/zenodo.7958708.

Acknowledgments
The authors would like to thank the Tribal Council and residents of Beaver, AK for access to their land and logistical support during fieldwork, in particular Liz Blackbird, Kody Vanderpool, Clinton Wiehl, Richard J. Williams, and Paul Williams Jr. We thank Rain Blankenship, Hannah Dion-Kirshner, Emily Geyman, Yutian Ke, John Magyar, Edda Mutter, Justin Nghiem, Jocelyn Reahl, Emily Seelen, Isabel Smith, A. Joshua West, and Lisa Winter for their assistance during fieldwork and two anonymous reviewers, whose recommendations greatly improved the manuscript. The authors acknowledge funding from NSF Awards 2127442, 2031532, and 2053009, Caltech's Resnick Sustainability Institute, and the National Defense Science and Engineering Graduate Fellowship.

References

Arenson, L. U., & Springman, S. M. (2005). Triaxial constant stress and constant strain rate tests on ice-rich permafrost samples. *Canadian Geotechnical Journal*, *42*(2), 412–430. https://doi.org/10.1139/t04-111

Beltaos, S., & Burrell, B. C. (2021). Effects of river-ice breakup on sediment transport and implications to stream environments: A review. *Water*, *13*(18), 2541. https://doi.org/10.3390/w13182541

Biskaborn, B. K., Lanckman, J.-P., Lantuit, H., Elger, K., Streletskiy, D. A., Cable, W. L., & Romanovsky, V. E. (2015). The new database of the Global Terrestrial Network for Permafrost (GTN-P). *Earth System Science Data*, *7*(2), 245–259. https://doi.org/10.5194/essd-7-245-2015

Bragg, R. A., & Andersland, O. B. (1981). Strain rate, temperature, and sample size effects on compression and tensile properties of frozen sand. *Engineering Geology*, *18*(1), 35–46. https://doi.org/10.1016/0013-7952(81)90044-2

Bronen, R., & Chapin, F. S. (2013). Adaptive governance and institutional strategies for climate-induced community relocations in Alaska. *Proceedings of the National Academy of Sciences of the United States of America*, *110*(23), 9320–9325. https://doi.org/10.1073/pnas.1210508110

Clement, D. T. (1999). *Fluvial geomorphology of the Yukon River, Yukon Flats, Alaska*. (Master of Science). University of Calgary.

Costard, F., Dupeyrat, L., Gautier, E., & Carey-Gailhardis, E. (2003). Fluvial thermal erosion investigations along a rapidly eroding river bank: Application to the Lena River (central Siberia). *Earth Surface Processes and Landforms*, *28*(12), 1349–1359. https://doi.org/10.1002/esp.592

Costard, F., Gautier, E., Fedorov, A., Konstantinov, P., & Dupeyrat, L. (2014). An assessment of the erosion potential of the fluvial thermal process during ice breakups of the Lena River (Siberia). *Permafrost and Periglacial Processes*, *25*(3), 162–171. https://doi.org/10.1002/ppp.1812

de Leeuw, J., Lamb, M. P., Parker, G., Moodie, A. J., Haught, D., Venditti, J. G., & Nittrouer, J. A. (2020). Entrainment and suspension of sand and gravel. *Earth Surface Dynamics*, *8*(2), 485–504. https://doi.org/10.5194/esurf-8-485-2020

Docherty, C. L., Dugdale, S. J., Milner, A. M., Abermann, J., Lund, M., & Hannah, D. M. (2019). Arctic river temperature dynamics in a changing climate. *River Research and Applications*, *35*(8), 1212–1227. https://doi.org/10.1002/rra.3537

Dupeyrat, L., Costard, F., Randriamazaoro, R., Gailhardis, E., Gautier, E., & Fedorov, A. (2011). Effects of ice content on the thermal erosion of permafrost: Implications for coastal and fluvial erosion. *Permafrost and Periglacial Processes*, *22*(2), 179–187. https://doi.org/10.1002/ppp.722

Fuchs, M., Nitze, I., Strauss, J., Günther, F., Wetterich, S., Kizyakov, A., et al. (2020). Rapid fluvio-thermal erosion of a yedoma permafrost cliff in the Lena River delta. *Frontiers of Earth Science*, *8*, 336. https://doi.org/10.3389/feart.2020.00336

Gordeev, V. V. (2006). Fluvial sediment flux to the Arctic Ocean. *Geomorphology*, *80*(1), 94–104. https://doi.org/10.1016/j.geomorph.2005.09.008

Kanevskiy, M., Shur, Y., Strauss, J., Jorgenson, T., Fortier, D., Stephani, E., & Vasiliev, A. (2016). Patterns and rates of riverbank erosion involving ice-rich permafrost (yedoma) in northern Alaska. *Geomorphology*, *253*, 370–384. https://doi.org/10.1016/j.geomorph.2015.10.023

Kean, J. W., & Smith, J. D. (2004). Flow and boundary shear stress in channels with woody bank vegetation. In *Riparian vegetation and fluvial geomorphology* (pp. 237–252). American Geophysical Union (AGU). https://doi.org/10.1029/008WSA17

Lininger, K. B., Wohl, E., Rose, J. R., & Leisz, S. J. (2019). Significant floodplain soil organic carbon storage along a large high-latitude river and its tributaries. *Geophysical Research Letters*, *46*(4), 2121–2129. https://doi.org/10.1029/2018GL080996

Lunardini, V. J. (1986). *Experimental determination of heat transfer coefficients in water flowing over a horizontal ice sheet*. (CRREL Report No. 86–3). US Army Corps of Engineers, Cold Regions Research & Engineering Laboratory.

McNamara, J. P., Oatley, J. A., Kane, D. L., & Hinzman, L. D. (2008). Case study of a large summer flood on the north slope of Alaska: Bedload transport. *Hydrology Research*, *39*(4), 299–308. https://doi.org/10.2166/nh.2008.006

Naito, K., & Parker, G. (2019). Can bankfull discharge and bankfull channel characteristics of an Alluvial meandering river be cospecified from a flow duration curve? *Journal of Geophysical Research: Earth Surface*, *124*(10), 2381–2401. https://doi.org/10.1029/2018JF004971

Naito, K., & Parker, G. (2020). Adjustment of self-formed bankfull channel geometry of meandering rivers: Modelling study. *Earth Surface Processes and Landforms*, *45*(13), 3313–3322. https://doi.org/10.1002/esp.4966

Obu, J., Westermann, S., Bartsch, A., Berdnikov, N., Christiansen, H. H., Dashtseren, A., et al. (2019). Northern Hemisphere permafrost map based on TTOP modelling for 2000–2016 at 1 km^2 scale. *Earth-Science Reviews*, *193*, 299–316. https://doi.org/10.1016/j.earscirev.2019.04.023

Parker, G. (1978). Self-formed straight rivers with equilibrium banks and mobile bed. Part 2. The gravel river. *Journal of Fluid Mechanics*, *89*(1), 127–146. https://doi.org/10.1017/S0022112078002505

Parker, G., Shimizu, Y., Wilkerson, G. V., Eke, E. C., Abad, J. D., Lauer, J. W., et al. (2011). A new framework for modeling the migration of meandering rivers. *Earth Surface Processes and Landforms*, *36*(1), 70–86. https://doi.org/10.1002/esp.2113

Parker, G., Toro-Escobar, C. M., Ramey, M., & Beck, S. (2003). Effect of floodwater extraction on mountain stream morphology. *Journal of Hydraulic Engineering*, *129*(11), 885–895. https://doi.org/10.1061/(ASCE)0733-9429(2003)129:11(885)

Partheniades, E. (1965). Erosion and deposition of cohesive soils. *Journal of the Hydraulics Division*, *91*(1), 105–139. https://doi.org/10.1061/JYCEAJ.0001165

Patsinghasanee, S., Kimura, I., Shimizu, Y., & Nabi, M. (2018). Experiments and modelling of cantilever failures for cohesive riverbanks. *Journal of Hydraulic Research*, *56*(1), 76–95. https://doi.org/10.1080/00221686.2017.1300194

Peterson, B. J., Holmes, R. M., McClelland, J. W., Vörösmarty, C. J., Lammers, R. B., Shiklomanov, A. I., et al. (2002). Increasing river discharge to the Arctic Ocean. *Science*, *298*(5601), 2171–2173. https://doi.org/10.1126/science.1077445

Rowland, J., Stauffer, S., & Schwenk, J. (2019). Pan-arctic river bank erosion and accretion, and planform metrics measured over intervals ranging from 1973 to 2016. Incorporating the Hydrological Controls on Carbon Cycling in Floodplain Ecosystems into Earth System Models (ESMs). https://doi.org/10.15485/1571527

Scott, K. M. (1978). *Effects of permafrost on stream channel behavior in Arctic Alaska*. (Geological Survey Professional Paper No. 1068) (p. 19). U.S. Geological Survey.

Sylvester, Z., Durkin, P., & Covault, J. A. (2019). High curvatures drive river meandering. *Geology*, *47*(3), 263–266. https://doi.org/10.1130/G45608.1

Turetsky, M. R., Abbott, B. W., Jones, M. C., Anthony, K. W., Olefeldt, D., Schuur, E. A., et al. (2020). Carbon release through abrupt permafrost thaw. *Nature Geoscience*, *13*(2), 138–143. https://doi.org/10.1038/s41561-019-0526-0

UAF, & USACE. (2019). *Statewide threat assessment: Identification of threats from erosion, flooding, and thawing permafrost in remote Alaska communities*. (No. INE 19.03) (p. 99). Denali Commission.

Vandermause, R., Harvey, M., Zevenbergen, L., & Ettema, R. (2021). River-ice effects on bank erosion along the middle segment of the Susitna river, Alaska. *Cold Regions Science and Technology*, *185*, 103239. https://doi.org/10.1016/j.coldregions.2021.103239

Wagner, A., Lohmann, G., & Prange, M. (2011). Arctic river discharge trends since 7 ka BP. *Global and Planetary Change*, *79*(1), 48–60. https://doi.org/10.1016/j.gloplacha.2011.07.006

Wanders, N., van Vliet, M. T. H., Wada, Y., Bierkens, M. F. P., & van Beek, L. P. H. (2019). High-resolution global water temperature modeling. *Water Resources Research*, *55*(4), 2760–2778. https://doi.org/10.1029/2018WR023250

Winterwerp, J. C., van Kesteren, W. G. M., van Prooijen, B., & Jacobs, W. (2012). A conceptual framework for shear flow–induced erosion of soft cohesive sediment beds. *Journal of Geophysical Research*, *117*(C10), C10020. https://doi.org/10.1029/2012JC008072

Wolfe, L. H., & Thieme, J. O. (1964). Physical and thermal properties of frozen soil and ice. *Society of Petroleum Engineers Journal*, *4*(01), 67–72. https://doi.org/10.2118/675-PA